

Synthesis of High Relaxivity Gadolinium AAZTA Tetramers as Building Blocks for Bioconjugation

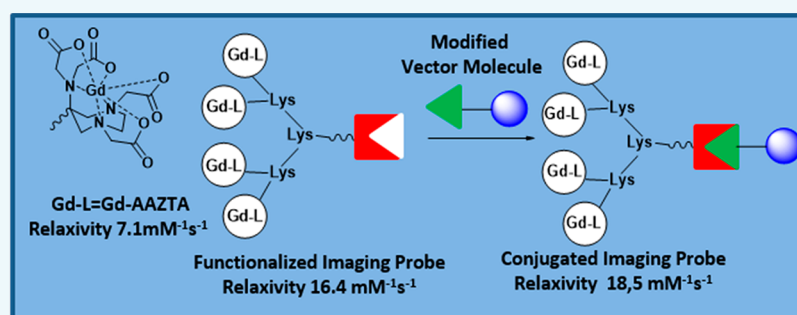
Martina Tripepi,[†] Federico Capuana,[†] Eliana Gianolio,[†] Flávio Vinicius Crizóstomo Kock,[‡] Amerigo Pagoto,[†] Rachele Stefania,^{*,†} Giuseppe Digilio,[§] and Silvio Aime[†]

[†]Department of Molecular Biotechnology and Health Sciences, University of Torino, Via Nizza 52, 10126-Torino, Italy

[‡]São Carlos Institute of Chemistry, São Paulo University, Av. Trabalhador São Carlense, 400, 13566-590, São Carlos, São Paulo, Brazil

[§]Department of Science and Technological Innovation, Università del Piemonte Orientale “A. Avogadro”, Viale T. Michel 11, 15121 Alessandria, Italy

S Supporting Information



ABSTRACT: Molecular imaging requires the specific accumulation of contrast agents at the target. To exploit the superb resolution of MRI for applications in molecular imaging, gadolinium chelates, as the MRI contrast agents (CA), have to be conjugated to a specific vector able to recognize the epitope of interest. Several Gd(III)-chelates can be chemically linked to the same binding vector in order to deliver multiple copies of the CA (multimers) in a single targeting event thus increasing the sensitivity of the molecular probe. Herein three novel bifunctional agents, carrying one functional group for the bioconjugation to targeting vectors and four Gd(III)-AAZTA chelate functions for MRI contrast enhancement (AAZTA = 6-amino-6-methylperhydro-1,4-diazepinetetraacetic acid), are reported. The relaxivity in the tetrameric derivatives is $16.4 \pm 0.2 \text{ mM}_{\text{Gd}}^{-1} \text{ s}^{-1}$ at 21.5 MHz and 25 °C, being 2.4-fold higher than that of parent, monomeric Gd(III)-AAZTA. These compounds can be used as versatile building blocks to insert preformed, high relaxivity, and high density Gd-centers to biological targeting vectors. As an example, we describe the use of these bifunctional Gd(III)-chelates to label a fibrin-targeting peptide.

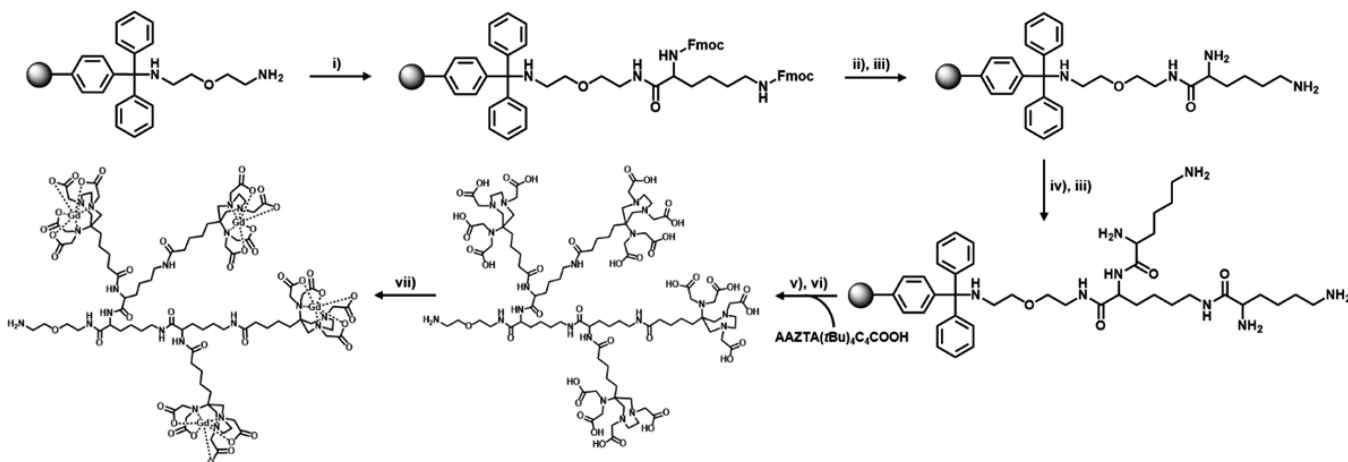
INTRODUCTION

Low-molecular-weight (LMW) Gd(III)-chelates are used as contrast agents (CAs) in about 40% of the magnetic resonance imaging (MRI) clinical scans worldwide. The efficacy of Gd(III)-complexes as MRI CAs is attributed to their ability to accelerate the water proton relaxation rate in tissues, adding valuable pathophysiologic contrast information to the inherent anatomic resolution of MR images. Besides the well-established applications of Gd-based chelates in clinical MRI, interesting perspectives are expected also in the field of diagnostic X-ray based computed tomography (CT) techniques. Spectral photon counting computed tomography (SPCCT) is a recent X-ray based medical imaging technique that allows the quantitation of electron-dense elements in a specific ROI by exploiting their specific K-edge absorption.¹ Gadolinium has been shown to have almost ideal physicochemical properties in terms of K-edge absorption energy and specific absorption coefficient to behave as a CA for SPCCT.^{2,3}

However, it is already clear that the new applications will rely on the attainment of high local concentrations of the Gd-containing systems. Currently, CAs used in the clinics are LMW Gd-chelates that extravasate specifically into tissues. Some of the clinically relevant LMW Gd-chelates contain hydrophobic groups that endow them with a high binding affinity to serum albumin, hence a prolonged lifetime in the bloodstream and suitable properties for angiographic applications (blood pool agents).^{4–6} It was soon realized that Gd-chelates could be functionalized with epitopes having high binding affinity and specificity for molecular targets other than albumin, paving the way to molecular imaging by MRI.^{7,8} Molecular imaging of biological targets requires the specific accumulation of suitable amounts of contrast agents at the target. However, the tissue density of the molecular target might be inherently low, and MRI has an intrinsically low

Received: February 15, 2018

Published: February 22, 2018

Scheme 1. Synthesis Scheme of Ligand L1 and Complex Gd-L1^{a,r}

^a(i) Fmoc-Lys(Fmoc)-OH 2.5 equiv, PyBOP and DIPEA in DMF; (ii) acetic anhydride-DMF 20%; (iii) 40% piperidine-DMF (5 min) and 20% piperidine-DMF (15 min); (iv) Fmoc-Lys(Fmoc)-OH 5 equiv, PyBOP and DIPEA in DMF; (v) AAZTA(tBu)₄C₄COOH 4.2 equiv, PyBOP and DIPEA in DMF; (vi) TFA, DCM, and TIS 49:49:2 (5 min, three times), and TFA 100% (12 h); (vii) GdCl₃ in water.

sensitivity as compared to other molecular imaging modalities, such as nuclear medicine (NM) or optical imaging (OI). As a consequence, MR molecular imaging applications may be hampered by the amount of CA that can be accumulated with a 1:1 gadolinium-to-target stoichiometric ratio.^{9,10}

An approach to increase the density of the contrast agent at the targeting sites is to link several Gd-chelates to the same binding vector in order to accumulate multiple copies of the CA in a single target binding event. This can be done by attaching a number of Gd-chelates to a scaffold with multimeric/dendrimeric structure, which must then be conjugated to the target binding vector.^{11,12} The target binding moieties used in MR molecular imaging belong to widely heterogeneous classes of chemical structures. Proteins, polypeptides, antibodies, DNA, polysaccharides, and lipids have been used as vectors.^{13,14} Often, the targeting vector is displayed on the surface of nanoparticles or liposomes.¹⁵ As the synthesis and/or purification of such systems can demand time and effort, it is of paramount importance to develop highly sensitive, multimeric Gd-chelates carrying functional groups for a prompt conjugation to the targeting vectors. The availability of such methods will provide molecular imaging scientists with a modular approach to easily assemble the needed imaging labeled targeted probe.

In this paper, we describe the synthesis of novel Gd-tetramers ending up with different functional groups ready for the bioconjugation to the targeting vectors. The selected metal chelator is the heptadentate AAZTA ligand (AAZTA = 6-amino-6-methylperhydro-1,4-diazepinetetraacetic acid). The [Gd(III)-AAZTA]⁻ complex (shortly, Gd-AAZTA) shows very good relaxivity properties (7.1 mM⁻¹ s⁻¹ at 21.5 MHz and 25 °C), as the heptadentate AAZTA chelator leaves room for two rapidly exchanging water molecules ($q = 2$, $\tau_M = 90$ ns) in the inner coordination sphere of Gd(III).¹⁶ Despite the relatively low denticity of AAZTA, the Gd-complex shows very good thermodynamic stability and kinetic inertness as compared to complexes with other octadentate polyaminocarboxylic ligands.¹⁷ Moreover, its mesocyclic structure should ensure a higher metabolic stability as compared to linear chelators.^{18,19} These properties²⁰ make Gd-AAZTA very attractive for clinical translation²⁰ and for the development of

dendrimers with enhanced relaxivity.^{21,22} Four AAZTA units were linked through amide bonds to a lysine-based dendrimer (dK₃), to obtain the AAZTA-tetramer (L1). The latter compound was functionalized with three different functional groups for conjugation, to obtain, namely, (i) compound L2, bearing the maleimide conjugation group able to react with free thiols to yield a thioester bond; (ii) compound L3, bearing an aromatic aldehyde able to react with an aromatic hydrazine-labeled molecule to yield a bis-aryl hydrazone-conjugate; (iii) compound L4 bearing a dibenzocyclooctyne (DBCO) moiety able to react with an azide-labeled molecule to yield a triazole conjugate via Cu(I)-free click chemistry.²³ The L2–4 ligands were complexed with Gd(III) ions to yield the corresponding Gd-tetramers (namely, Gd-L2, Gd-L3, and Gd-L4), ready for bioconjugation. As an example, the protocol for conjugation of the Gd-L2 tetramer to a fibrin-targeting peptide is also reported.

RESULTS AND DISCUSSION

Design, Synthesis, and Characterization. Ligand L1 was designed to contain a single free amino group at the end of a spacer for further conjugation with a range of functional groups. Four AAZTA-units were connected to form a tetrameric compound through a branched trilycine scaffold. The spacer and the trilycine scaffold are expected to ensure a high flexibility within the tetramer structure. Such a flexibility is sought for minimizing steric hindrance issues with regard to the conjugation reaction to targeting vectors. Moreover, flexibility of the MRI label and suitable spacing from the targeting vector are also thought to minimize possible interference in the molecular recognition of the biological target. As a drawback of such flexibility, some limitation to the attainable relaxivity may also be expected.

To synthesize precursor L1 (Scheme 1), the bis(2-aminoethyl)-ether trityl resin and 9-fluorenylmethoxycarbonyl (Fmoc) protection chemistry were chosen for the setup of solid phase peptide synthesis (SPPS) approach. After coupling the first lysine residue (under the form of N α ,N ϵ -di-Fmoc-L-lysine) to the resin, the resin was treated with acetic anhydride in DMF to acetylate the residual free amino groups exposed on its surface. Then, after removal of the Fmoc group by adding

20% piperidine in DMF, two more lysine residues were attached. The coupling reactions were performed with 2.5-fold excess Fmoc-Lys(Fmoc)-OH, dissolved in DMF, with PyBOP and DIPEA as the activators, following Fmoc deprotection. The branched trilycine core anchored on the resin provided four amino groups (two α -amino and two side-chain amino groups) that were used to synthesize the tetrameric AAZTA-based ligand **L1**. The latter coupling was performed with a small excess of the AAZTA derivative AAZTA(*t*Bu)₄C₄COOH (Figure 1), whose synthesis has been described previously.²⁴

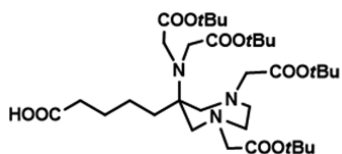


Figure 1. Structure of the AAZTA derivative AAZTA(*t*Bu)₄C₄COOH.

The coupling reaction between AAZTA and the trilycine scaffold turned out to be a tricky step, as the final yield was strongly dependent upon the activating agent. PyBOP was found to be the most efficient activator for this synthetic step. After cleavage from the resin and purification by semi-preparative HPLC, an overall yield of about 60% and purity of 98% of **L1** were obtained.

When HBTU was used instead of PyBOP, a decrease of the yield by 30% and a higher amount of a side-product containing only three AAZTA units coupled to the lysine scaffold was found. This impurity arises from the transfer of a tetramethyluronium moiety from HBTU to the amino group, with the formation of a stable tetramethylguanidine derivative.²⁵ Such a side reaction is likely favored by the high density

of the amino groups in the trilycine scaffold and by the slow rate of coupling of the fourth AAZTA unit due to an increasing steric hindrance. Besides the decrease of the final yield, the formation of such an impurity induced problems in the purification step by semi-preparative reverse phase HPLC. The impurity gave a characteristic signal at 2.90 ppm in ¹H NMR spectra (Figure 2) and characteristic ESI+ MS peaks at *m/z* 938.6 [M+2H]²⁺ and 625.9 [M+3H]³⁺, corresponding to the molecular formula C₈₁H₁₃₉N₁₉O₃₁.

The amine end-group in the molecular structure of **L1** was easily converted to maleimide (**L2**), benzaldehyde (**L3**), or cyclooctyne (**L4**) by reacting the **L1** ligand with a 3-fold molar excess of *N*-succinimidyl-3-maleimido propionate, or *N*-succinimidyl-4-formylbenzoate, or dibenzocyclooctyne-*N*-hydroxysuccinimidyl ester, respectively, in phosphate buffer 50 mM and CH₃CN 3:1. HPLC-MS (ESI+) analysis indicated a total conversion of **L1** into the **L2**, **L3**, or **L4** compounds (Scheme 2). The excess reagents and salts were removed by size exclusion chromatography, without a significant loss of the product. The fully assigned NMR spectra and HPLC-UV/MS (ESI+) chromatograms of ligands **L2**, **L3**, and **L4** are reported in the Supporting Information.

The Gd^{III} complexes were prepared by mixing stoichiometric amounts (1:4) of the AAZTA-tetramer and GdCl₃ solution. While this step occurred without any problem for **L1**, **L3**, and **L4**, a substantial loss of **L2** may take place because of the hydrolysis of the maleimide group. However, we have found that complete complex formation can be attained, within 1 h reaction, when the pH is carefully maintained at 6.5 (with the additions of NaOH).

As an example of practical application, we applied our bifunctional agent to label a fibrin-binding peptide. We chose the EP-2104R fibrin-binding peptide (FibPep), that was

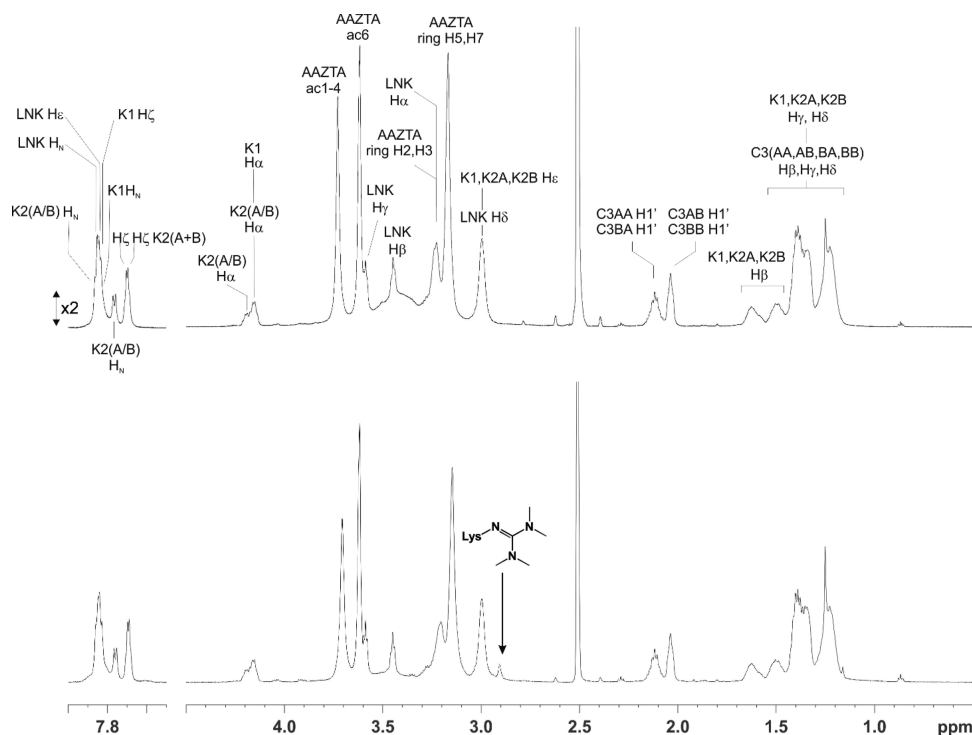
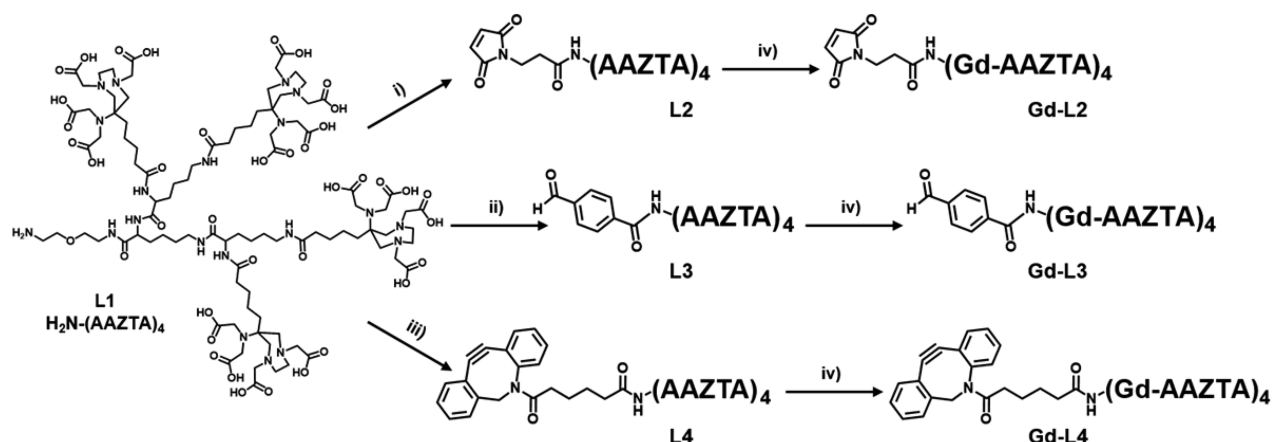


Figure 2. ¹H NMR spectrum of **L1** synthesized by using PyBOP (top) or HBTU (bottom) as the activator in SPPS, after purification by RP-HPLC. The arrow marks the signal at 2.90 ppm of the side product arising from the transfer of a tetramethyluronium group from HBTU to one lysine, yielding a tetramethylguanidine. See Supporting Information for full assignment of the ¹H NMR spectrum of **L1** and atom nomenclature.

Scheme 2. Synthesis of Ligands Bearing Functional Groups for Bioconjugation (L2, L3, and L4) and of Their Gd(III)-Complexes (Gd-L2, Gd-L3, and Gd-L4)^a



^a(i) *N*-Succinimidyl-3-maleimido propionate (3 equiv) in buffer phosphate 50 mM at pH 7 and CH₃CN; (ii) *N*-succinimidyl-4-formylbenzoate (3 equiv) in buffer phosphate 50 mM at pH 7 and CH₃CN; (iii) dibenzocyclooctyne-*N*-hydroxysuccinimidyl ester (3 equiv) in buffer phosphate 50 mM at pH 7 and CH₃CN; (iv) GdCl₃ in water.

originally introduced and comprehensively characterized by Caravan and co-workers.^{26,27} Fibrin targeting with paramagnetic agents has an outstanding diagnostic potential, as fibrin is a major component of blood clots and plays an important role in thrombi-related pathologies such as deep venous thrombosis, pulmonary embolism, and atherosclerosis. In fact, several examples of peptide-based fibrin targeted molecular probes have been reported.^{28–30} FibPep is a cyclic 11-amino-acid peptide that showed significantly higher binding to fibrin than other reported peptides. The peptide was synthesized on Rink amide 4-methylbenzhydrylamine using standard Fmoc solid-phase peptide synthesis. FibPep was modified with a glycine at the C-terminal and with two glycines at the N-terminal as spacers and then conjugated to **Gd-L2** through the thiol/maleimide chemistry. Thus, *N*-succinimidyl-*S*-acetylthioacetate (SATA) was reacted to the N-terminal and then the peptide cleaved from the resin. Disulfide bridge was then formed between Cys5 and Cys10 and the acetylthio group was removed using hydroxylamine. Finally, the thiol-bearing peptide was reacted with the maleimide of **Gd-L2** at a molar ratio of 1:1 at pH 6.5 to yield the Gd-labeled peptide (**FibPep-Gd-L2**) in 80% yield. It is worth emphasizing that, by applying this procedure, Gd-chelates are directly conjugated to the targeting vector, contrary to the typical two-step approach that involves the conjugation of the chelator and then complexation with gadolinium. Thus, the approach presented herein eliminates the “free” gadolinium issue (i.e., Gd(III) ions being weakly coordinated to the secondary coordinating sites potentially offered by the peptidic structure).^{31–33} This approach may be particularly useful when the targeting vector has the chemical complexity of proteins, antibodies, and polysaccharide-based systems.

Relaxivity. The **Gd-L1** complex showed a relaxivity, in water, of $16.4 \pm 0.2 \text{ mM}_{\text{Gd}}^{-1} \text{ s}^{-1}$ (0.5 T, 25 °C). It is significantly higher than that of monomeric Gd-AAZTA ($7.1 \text{ mM}^{-1} \text{ s}^{-1}$),¹⁶ resulting in an overall relaxivity per molecule of $65.6 \pm 0.8 \text{ mM}^{-1} \text{ s}^{-1}$. The nuclear magnetic resonance dispersion (NMRD) profile of **Gd-L1** (Figure 3, Table 1) as compared to that of Gd-AAZTA shows higher relaxivities throughout the magnetic field strength studied and a smooth relaxivity peak centered at around 40–50 MHz.

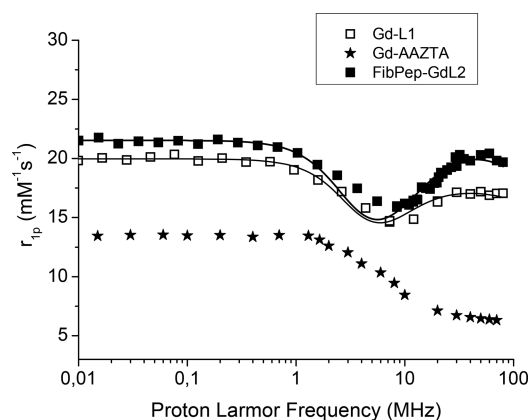


Figure 3. NMRD profiles of **Gd-L1** (□) and **FibPep-Gd-L2** (■) compared to those of Gd-AAZTA (★). Experimental data points were measured on 1 mM aqueous solutions of the Gd-complexes at 298 K, pH = 7. Lines are best fitting to the theory.

This profile is consistent with an increase of the reorientational correlation time, τ_R , expected on the basis of the increased molecular size due to the tetrameric structure (macromolecule effect). However, the relaxivity is not as high as one could expect on the basis of the size of the tetrameric system. In fact, the observed relaxivity is well below the straight line obtained by plotting the relaxivity of known Gd(III) complexes, with two inner sphere water molecules, versus their molecular weight (Figure 4).

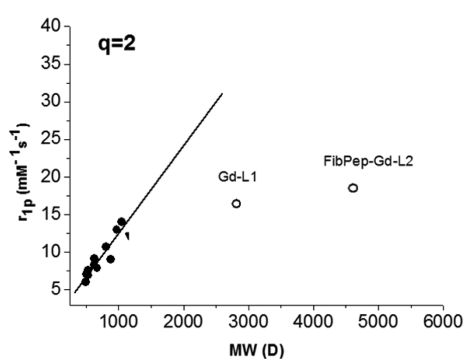
This can be ascribed to relatively fast internal motions that partially decouple the reorientation of each of the four Gd-AAZTA chelates from the overall global tumbling motion. To get further insights, a quantitative view of the parameters governing the relaxivity of **Gd-L1** has been obtained by multiparametric fitting of the NMRD profile according to the Solomon–Bloembergen–Morgan (SBM) theory for inner sphere paramagnetic relaxation, combined with the Freed theory for outer sphere paramagnetic relaxation,⁴¹ and modified according to the Lipari-Szabo model-free approach for the description of the rotational dynamics.⁴² This model allows one to take into account the presence of a certain degree of internal motions superimposed on the overall tumbling motion. These

Table 1. Main Parameters Derived from Fitting of NMRD Profiles Reported in Figure 3^a

system	r_{1p} ($\text{mM}_{\text{Gd}}^{-1} \text{s}^{-1}$)	Δ^{2b} (s^{-2})	τ_V^c (ps)	τ_{RI}^d (ps)	τ_{Rg}^e (ps)	S^2
Gd-L1	16.4 ± 0.2	$(1.89 \pm 0.97) \times 10^{19}$	36.3 ± 3.50	309 ± 63	741 ± 116	0.068
FibPep-Gd-L2	18.5 ± 0.3	$(2.08 \pm 0.15) \times 10^{19}$	30.9 ± 1.49	305 ± 58	1080 ± 310	0.087

^aOn carrying out the fitting procedure, the following parameters were kept fixed: $r_{\text{Gd-H}}$ (distance between Gd and protons of the inner sphere water molecule) = 3.1 Å; a (distance of minimum approach of solvent water molecules to Gd^{3+} ion) = 3.8 Å; D (solvent diffusion coefficient) = $2.2 \times 10^{-5} \text{ cm}^2 \text{ s}^{-1}$. ^bSquared mean transient zero-field splitting (ZFS) energy. ^cCorrelation time for the collision-related modulation of the ZFS Hamiltonian.

^dReorientational correlation time, local motions. ^eReorientational correlation time, global motions.



Gd-complex	MW (D)	r_{1p} (0.47T, 25°C)	ref
Gd-DO3A	500	6,0	34
Gd-AAZTA	514	7,1	16
Gd-L1a	530	7,6	35
Gd-PCTA[12]	534	6,9	36
Gd-PCTA[12]Bz	625	8,3	37
Gd-L2	629	9,1	35
Gd-BrDO3A	672	7,9	38
Gd-PPDO3A	808	10,7	38
Gd-TREN-Me-3,2 HOPO	880	9,0	39
B25716	974	13,0	40
(Gd-AAZTA) ₂	1049	14,0	22
Gd-L1	2820	16,4	this work
FibPep-Gd-L2	4614	18,5	this work

Figure 4. Molecular weight (MW) dependence of the relaxivity (0.47 T, 298 K) for typical Gd(III) complexes with two inner-sphere water molecules. Data points have been interpolated by linear regression: $r_{1p} = 0.011\text{MW} + 0.928$ ($r^2 = 0.815$).^{34,16,35–40,22}

Table 2. Relaxivity per Gadolinium ($\text{mM}_{\text{Gd}}^{-1} \text{s}^{-1}$) of the Different Gd-Tetrameric Systems Measured at 0.5, 1, and 1.5 T and 25 and 37 °C in Water and in Serum^a

system	water		serum					
	0.5 T		0.5 T		1 T		1.5 T	
	25 °C	37 °C	25 °C	37 °C	25 °C	37 °C	25 °C	37 °C
Gd-L1	16.4 ± 0.2	12.5 ± 0.1	18.8 ± 0.2	14.6 ± 0.2	19.5 ± 0.2	15.1 ± 0.1	19.5 ± 0.1	15.3 ± 0.1
Gd-L2	16.0 ± 0.2	12.5 ± 0.1	17.6 ± 0.2	13.7 ± 0.1	-	-	-	-
Gd-L3	16.8 ± 0.2	12.8 ± 0.2	18.3 ± 0.2	14.1 ± 0.2	-	-	-	-
Gd-L4	16.6 ± 0.2	12.6 ± 0.1	21.0 ± 0.2	16.7 ± 0.2	-	-	-	-
FibPep-Gd-L2	18.5 ± 0.3	14.3 ± 0.1	22.5 ± 0.2	18.5 ± 0.2	23.2 ± 0.2	18.7 ± 0.2	21.6 ± 0.2	16.9 ± 0.2

^aRelaxation rate measurements were carried out on 1 mM gadolinium solutions, pH = 7.

two types of motions, a relatively fast local rotation of the coordination cage, superimposed on the global reorientation of the system, are characterized by different correlation times, namely, τ_{RI} and τ_{Rg} , respectively. The degree of correlation between global and local rotations is given by the parameter S^2 , which takes values between zero (completely independent motions) and one (entirely correlated motions). Such analysis yielded correlation times for both the local and the global motion that are significantly increased as compared to the τ_{R} value of parent monomeric Gd-AAZTA (74 ps; see Table 1). However, the S^2 value is very low ($S^2 = 0.068$) as a consequence of the great flexibility of the Gd-coordination cages around the linkers that interconnect the four AAZTA chelating units. The relaxivity values of Gd-L2, Gd-L3, Gd-L4 were very similar to those of Gd-L1 (Table 2).

The relaxivity of FibPep-Gd-L2, at 0.5 T in water and 25 °C, was $18.5 \pm 0.3 \text{ mM}_{\text{Gd}}^{-1} \text{ s}^{-1}$ ($74 \pm 1 \text{ mM}^{-1} \text{ s}^{-1}$ per molecule). Upon increasing the temperature (Table 2), the relaxivity of all the tetramers decreases as expected on the basis of a shortening of the overall molecular tumbling time. When measured in serum, the observed relaxivities were slightly higher than in water, likely as a consequence of the increased viscosity. More

important, on passing from water to serum the absence of any “quenching” of the observed relaxivity is indicative of the inability of the endogenous anions (e.g., phosphates, carbonates, etc.) to replace the two water molecules in the inner coordination sphere. Thus, the tetrameric derivatives maintain this relevant property of the parent Gd-AAZTA complex.¹⁶ In the case of Gd-L1 and FibPep-Gd-L2, the relaxivity values were measured also at field strength values more relevant for clinical applications (1 and 1.5 T). At both 25 and 37 °C the relaxivity slightly increases by increasing the magnetic field in the range 0.5–1.5 T. This favorable behavior is frequently associated with systems endowed with intermediate molecular weight characteristics.^{43,44}

Fibrin Binding. The affinity of the peptide–tetramer conjugate to fibrin was tested by an adaptation of a well-established methodology,²⁶ that relies on the thrombin-induced formation of fibrin clots from plasma fibrinogen, in the presence of the binding peptide. The concentration of FibPep-Gd-L2 bound to the clot was obtained by isolating the clot from the plasma supernatant and determining the concentration of gadolinium by ICP-MS analysis (see Materials

and Methods). The data were fit to the classical model for drug–receptor binding (eq 1)

$$[\text{FibPep-Gd-L2}]_{\text{bound}} = \frac{B_{\text{max}} \times [\text{FibPep-Gd-L2}]_{\text{free}}}{[\text{FibPep-Gd-L2}]_{\text{free}} + K_{\text{d}}} \quad (1)$$

where B_{max} is the maximum binding capacity, $[\text{FibPep-Gd-L2}]_{\text{free}}$ is the free Gd-tetramer concentration (μM), and K_{d} is the dissociation constant (μM). The binding curve reported in Figure 5 displays an unusual course. While the initial part of the

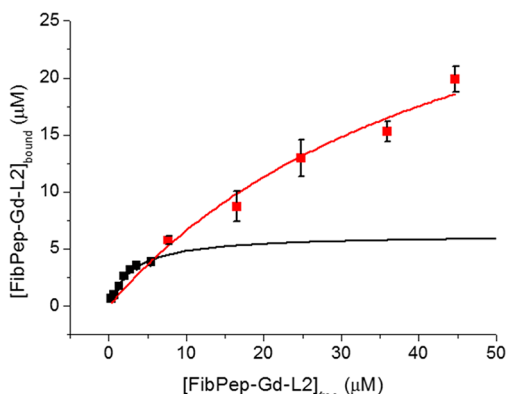


Figure 5. FibPep-Gd-L2 binding to fibrin clots from human plasma. Solid lines are the fitting curves as described in the text. Data are reported as mean \pm SD from three independent experiments.

curve is typical of specific binding, the final part does not reach a plateau as expected. Instead, the amount of bound FibPep-Gd-L2 keeps on increasing with increasing FibPep-Gd-L2 concentration in the incubation medium. The overall behavior is indicative of unspecific binding going on together with specific binding. Fitting of the first part of the curve yields a strong affinity constant ($K_{\text{d}} = 3.0 \pm 0.6 \mu\text{M}$, $B_{\text{max}} = 6 \pm 1$). However, when the full curve is considered for fitting, lower affinity binding sites are found ($K_{\text{d}} = 48 \pm 14 \mu\text{M}$) with a larger binding capacity ($B_{\text{max}} = 39 \pm 3$). The affinity of FibPep-Gd-L2 for fibrin is slightly lower than, but comparable to, that found for systems in which the same binding peptide was conjugated to four Gd-DOTAGA²⁶ or GdDTPA³⁵ complexes.

Finally, the relaxivity of FibPep-Gd-L2 in the fibrin plasma clots was determined at 25 °C and 0.5 T. The relaxivity per gadolinium was $58 \pm 13 \text{ mM}_{\text{Gd}}^{-1} \text{ s}^{-1}$ (mean \pm SD value of 3 experiments), which is $\sim 150\%$ higher than that measured in serum (Table 2). However, it must be considered that the high relaxivity found in clots arises from both specifically and aspecifically bound species, whose relative contribution to the observed relaxivity cannot be unambiguously disentangled. We speculate that the relaxivity of the aspecifically bound species might be significantly higher than that of the free species, because of the high microviscosity envisaged within the clot microenvironment. This matter certainly needs further investigation. With this limitation in mind, we observe that the $\sim 150\%$ relaxivity enhancement found for our $q = 2$ FibPep-Gd-L2 is comparable to that of EP-2104-R.²⁶ The latter is a $q = 1$ system based on the same target-binding peptide, but bearing four Gd-DOTA-like units. Thus, we envisage that the expected relaxivity loss (in the 20–60 MHz range) due to the high flexibility of Gd(III)-AAZTA chains is compensated by the combined effect of $q = 2$ hydration number and slow dynamics within the clot.

CONCLUSION

In conclusion, we have presented a protocol for the synthesis of three bifunctional agents, carrying one functional group for bioconjugation to targeting vectors and four Gd-AAZTA like functions as the MRI contrast agent. Despite the high internal flexibility of the Gd(III)-tetramer, the relaxivity per gadolinium shows a 2.4-fold increase as compared to that of monomeric Gd-AAZTA, due to the macromolecular effect. These compounds can be used as building blocks to insert preformed, high-relaxivity, and high-density Gd-centers to biological targeting vectors.¹⁶

MATERIALS AND METHODS

Bis(2-aminoethyl)-ether trityl resin, Fmoc-Lys(Fmoc)-OH, and activators HBTU and PyBOP were purchased from Novabiochem (Darmstadt, Germany). All other chemicals were purchased from Sigma-Aldrich. NMR spectra were recorded at 310 K on a Bruker AVANCE 600 spectrometer. Mass spectra with electrospray ionization (ESI) were recorded on a SQD 3100 Mass Detector (Waters). The HPLC-MS analytical and preparative analysis were carried out on a Waters AutoPurification system (3100 Mass Detector, 600 Quaternary Pump Gradient Module, 2767 Sample Manager, and 2487 UV/Visible Detector). UPLC analysis was performed using a UPLC Acquity H-Class coupled with the QDa and TUV Detectors. All ligands were characterized by NMR on a Bruker AVANCE 600 NMR spectrometer operating at 14T (corresponding to 600 and 150 MHz ¹H and ¹³C Larmor frequencies, respectively). The purified ligands L1–4 were freeze-dried from water solution at pH 2–3 and the powder redissolved in DMSO-*d*₆ for NMR analysis. Either homonuclear (2D-TOCSY, 2D-COSY, 2D-NOESY) or heteronuclear (2D-¹H,¹³C HSQC, 2D-¹H,¹³C HMBBC) two-dimensional NMR experiments were acquired to assign the spectra and confirm the structure of the ligands.

Synthesis of L1. Bis(2-aminoethyl)-ether trityl resin (0.96 mmol; 1.95 g) was loaded into a reaction vessel and dimethylformamide (DMF) (25 mL) was added to swell it for about 10 min. After the elimination of DMF, a mixture of Fmoc-Lys(Fmoc)-OH (2.39 mmol; 1.41 g), PyBOP (2.39 mmol; 1.24 g), and DIPEA (4.78 mmol; 0.83 mL) in DMF (20 mL) was added in the reactor and shaken for 1 h. The amino acid solution was then removed and 20% acetic anhydride–DMF (20 mL) was added and shaken for 15 min. The resin was washed five times with DMF and then the deprotection of the amino groups from Fmoc was done using 40% piperidine–DMF (20 mL) for 5 min and 20% piperidine–DMF (20 mL) for 15 min. After washing five times with DMF, the coupling cycle was repeated using a double quantity of Fmoc-Lys(Fmoc)-OH (4.78 mmol; 2.82 g), PyBOP (4.78 mmol; 2.49 g), and DIPEA (9.55 mmol; 1.67 mL) in DMF (20 mL), and the reaction was carried out again for 1 h, followed by DMF washing and piperidine treatment. After washing with DMF, a mixture of AAZTA(*t*Bu)₄C₄COOH²⁴ (4.02 mmol; 2.7 g), PyBOP (4.01 mmol; 2.09 g) and DIPEA (8.02 mmol; 1.40 mL) in DMF (20 mL) was added to the reactor and it was shaken for 1 h. The resin was washed five times with DMF and then thrice with dichloromethane (DCM). Afterward, diethyl ether (Et₂O) was used to completely dry the resin before the cleavage. A cocktail solution of DCM, trifluoroacetic acid (TFA), and triisopropylsilane (TIS) in a ratio 49:49:2 (10 mL) was added in the reactor and it was shaken for 5 min. The

solution was collected in a round-bottom flask and the process was repeated three times. Then the combined filtrate was reduced almost to dryness and fresh TFA was added and stirred overnight until the complete removal of *t*Bu of AAZTA. The mixture was then concentrated in vacuo and cold Et₂O (30 mL) was added to let the product precipitate. The precipitate was centrifuged and washed thrice with Et₂O. The crude product was dissolved in 5 mL of water and purified by preparative RP-HPLC using a Waters XTerra prep RPdC8, 5 μm, 19 × 100 mm column by Method 1 and H₂O/0.1% TFA (A) and CH₃CN/0.1% TFA (B) as eluents (see the [Supporting Information](#)). The volume of injection was 600 μL for every run and the desired product was fractioned, collected, and freeze-dried overnight. The pure product was obtained as a white powder (1.2 g, 57% of yield). The purity of the L1 was evaluated by analytical HPLC using XTerra RPdC8, 5 μm, 4.6 × 150 mm column, by Method 2 and H₂O/0.1% TFA (A) and CH₃CN/0.1% TFA (B) as eluents: a retention time of 5.84 min and a degree of purity of 98.7% of L1 were estimated (λ = 220 nm) (see the [Supporting Information](#)).

ESI-MS (*m/z*): [M+2H]²⁺ 1104.0 (obsd.), 1104.0 (calcd. for C₉₄H₁₅₆N₂₀O₄₀); [M+3H]³⁺ 736.3 (obsd.), 736.4 (calcd.); [M+4H]⁴⁺ 552.6 (obsd.), 552.6 (calcd.).

¹H NMR (600 MHz, DMSO-*d*₆, *T* = 310 K): 12.20 (*br*), 7.88 (5H, *o, m*), 7.79 (2H, *d*), 7.73–7.72 (2H, *o, m*), 4.22–4.19 (3H, *o, m*), 3.78 (16H, *s*), 3.65 (16H, *o, s*), 3.62 (2H, *o, t*), 3.48 (2H, *t*), 3.27 (18H, *o, m*), 3.20 (16H, *o, br*), 3.02 (8H, *o, m*), 2.15 (4H, *o, m*), 2.07 (4H, *o, m*), 1.66–1.53 (6H, *o, m*), 1.44–1.25 (36H, *o, m*).

Synthesis of L2, L3, and L4. To a solution of L1 (0.02 mmol; 50 mg) in buffer phosphate (50 mM; 3 mL; pH 7) was added *N*-succinimidyl-3-maleimido propionate (0.06 mmol; 16 mg) or *N*-succinimidyl-4-formylbenzoate (0.06 mmol; 15 mg) or dibenzocyclooctyne-*N*-hydroxysuccinimidyl ester (0.06 mmol; 24 mg) dissolved in 1 mL of CH₃CN for compound L2, L3, and L4, respectively. After stirring 4 h at RT, the organic phase was evaporated and the excess nonbound reagent and buffer products were removed by size exclusion chromatography on a HiTrap Desalting Column 5 mL prepacked with Sephadex G25, using Milli-Q H₂O as the mobile phase, after which the fractions corresponding to the functionalized product were collected. The L2, L3, and L4 compounds were checked with ESI-MS(+) and freeze-dried, obtaining about 70% of yield. The purity of the modified ligands was evaluated by analytical HPLC using XTerra RPdC8, 5 μm, 4.6 × 150 mm column, by Method 2, and H₂O/0.1% TFA (A) and CH₃CN/0.1% TFA (B) as eluents (see the [Supporting Information](#)).

L2. ESI-MS (*m/z*): [M+2H]²⁺ 1179.6 (obsd.), 1179.7 (calcd. for C₁₀₁H₁₆₁N₂₁O₄₃); [M+3H]³⁺ 786.8 (obsd.), 786.8 (calcd.); [M+4H]⁴⁺ 590.6 (obsd.), 590.2 (calcd.). Retention time 9.90 min, purity 90.0%.

¹H NMR (600 MHz, DMSO-*d*₆, *T* = 310 K): 12.20 (*br*), 8.03 (1H, *t*), 7.94–7.85 (4H, *o, m*), 7.83 (1H, *d*), 7.80–7.73 (2H, *o, m*), 7.00 (2H, *s*), 4.22–4.13 (3H, *o, m*), 3.85–3.75 (16H, *o, s*), 3.61–3.43 (18H, *o, br*), 3.41–3.35 (4H, *o, m*), 3.34–3.27 (18H, *o, m*), 3.23 (16H, *s*), 3.19–3.14 (2H, *o, m*), 2.99 (6H, *o, m*), 2.37 (2H, *t*), 2.15 (4H, *o, m*), 2.07 (4H, *o, m*), 1.66–1.53 (6H, *o, m*), 1.44–1.25 (36H, *o, m*).

L3. ESI-MS (*m/z*): [M+2H]²⁺ 1170.0 (obsd.), 1170.0 (calcd. for C₁₀₂H₁₆₀N₂₀O₄₂); [M+3H]³⁺ 780.5 (obsd.), 780.5 (calcd.); [M+4H]⁴⁺ 585.8 (obsd.), 585.5 (calcd.). Retention time 10.05 min, purity 93.3%.

¹H NMR (600 MHz, DMSO-*d*₆, *T* = 310 K): 12.20 (*br*), 10.10 (1H, *s*), 8.81 (1H, *t*), 8.08 (2H, *d*), 7.99 (2H, *d*), 7.95–7.86 (4H, *o, m*), 7.85 (1H, *d*), 7.80–7.75 (2H, *o, m*), 4.22–4.13 (3H, *o, m*), 3.85–3.75 (16H, *o, s*), 3.63 (16H, *o, s*), 3.57 (2H, *t*), 3.48 (2H, *o, m*), 3.45 (2H, *o, m*), 3.33–3.27 (18H, *o, m*), 3.23 (16H, *s*), 2.99 (6H, *o, m*), 2.15 (4H, *o, m*), 2.07 (4H, *o, m*), 1.66–1.53 (6H, *o, m*), 1.44–1.25 (36H, *o, m*).

L4. ESI-MS (*m/z*): [M+2H]²⁺ 1261.6 (obsd.), 1261.9 (calcd. for C₁₁₅H₁₇₃N₂₁O₄₂); [M+3H]³⁺ 841.5 (obsd.), 841.6 (calcd.); [M+4H]⁴⁺ 631.6 (obsd.), 631.4 (calcd.). Retention time 18.47 min, purity 90.1%.

¹H NMR (600 MHz, DMSO-*d*₆, *T* = 310 K): 12.20 (*br*), 8.01 (1H, *t*), 7.98–7.83 (6H, *o, m*), 7.80–7.74 (1H, *o, m*), 7.66 (1H, *d*), 7.59 (1H, *d*), 7.52 (1H, *t*), 7.51–7.46 (2H, *o, m*), 7.42 (1H, *t*), 7.38 (1H, *t*), 7.32 (1H, *d*), 5.08 (2H, *d*), 4.24–4.18 (3H, *br, o*), 3.87 (16H, *o, br*), 3.66 (16H, *o, s*), 3.43–3.37 (18H, *o, m*), 3.36–3.29 (18H, *o, s*), 3.25–3.13 (4H, *o, m*), 3.02 (6H, *o, m*), 2.22–2.13 (6H, *o, m*), 2.07 (4H, *o, t*), 1.91 (2H, *t*), 1.79 (2H, *m*), 1.66–1.53 (6H, *o, m*), 1.44–1.25 (38H, *o, m*).

Synthesis of Gd(III)-Complexes (Gd-L1, Gd-L2, Gd-L3, and Gd-L4). An equimolar amount of GdCl₃ (170 mM water solution) was slowly added to a 60 mM ligand solution; the solutions were maintained at pH 6.5 with NaOH. The complexes were then desalted by size exclusion chromatography on a HiTrap Desalting Column 5 mL prepacked with Sephadex G25, using Milli-Q H₂O as the mobile phase, and finally freeze-dried. The amount of residual free Gd³⁺ ions was assessed by the Orange Xylenol UV method.⁴⁶ All complexes were found to contain less than 0.3% (mol/mol) of residual free Gd³⁺ ions. The purity of Gd complexes was evaluated by analytical UPLC using ACQUITY UPLC Peptide BEH C18 Column, 1.7 μm, 2.1 mm × 150 mm by Method 3 for Gd-L2 and Gd-L3 and Method 4 for Gd-L4, using H₂O/0.05% TFA (A) and CH₃CN/0.05% TFA (B) as eluents (see the [Supporting Information](#)). All the derivatives were obtained in high purity, >90% (see the [Supporting Information](#)).

Gd-complexes were also analyzed by direct infusion in ESI-MS in negative-ion mode after dilution in CH₃OH–H₂O (50/50).

Gd-L1. ESI-MS *m/z*: [M-2H]²⁻ 1410.9 (obsd.), 1410.3 (calcd. for C₉₄H₁₄₀Gd₄N₂₀O₄₀); [M-3H]³⁻ 940.0 (obsd.), 939.5 (calcd.); [M-4H]⁴⁻ 704.8 (obsd.), 704.1 (calcd.).

Gd-L2. ESI-MS *m/z*: [M-3H]³⁻ 990.8 (obsd.), 990.9 (calcd. for C₁₀₁H₁₄₉Gd₄N₂₁O₄₃); [M-4H]⁴⁻ 742.7 (obsd.), 742.9 (calcd.).

Gd-L3. ESI-MS *m/z*: [M-3H]³⁻ 984.5 (obsd.), 984.5 (calcd. for C₁₀₂H₁₄₈Gd₄N₂₀O₄₂); [M-4H]⁴⁻ 737.7 (obsd.), 738.4 (calcd.).

Gd-L4. ESI-MS *m/z*: [M-3H]³⁻ 1045.4 (obsd.), 1045.6 (calcd. for C₁₁₅H₁₆₁Gd₄N₂₁O₄₂); [M-4H]⁴⁻ 783.7 (obsd.), 783.9 (calcd.).

Synthesis of FibPep. The peptide sequence GGY-dGlu-C-Hyp-3CIY-GLCYIQG, containing the fibrin binding motif, was synthesized by standard Fmoc solid-phase peptide synthesis on Rink amide 4-methylbenzhydrylamine resin and using a Liberty CEM microwave synthesizer. The coupling reactions were performed with 5.0 equiv excess of Fmoc-amino acids, 5 min at 75 °C, 35 W, in the presence of PyBOP and DIPEA in DMF, and the Fmoc-deprotection steps (20% piperidine in DMF) were completed within 3 min at 75 °C. At the end of the last cycle, the synthesized peptide was reacted with 2.5-fold excess of *N*-succinimidyl-S-acetylthioacetate (SATA) in DMF and stirring at RT for 3 h. A cocktail solution of TFA, H₂O, Phenol,

and TIS in a ratio 88:5:5:2 (v/v/wt/v, 15 mL) was used to cleave the peptide from the resin and to obtain the side-chain deprotection. After 3 h, the cleavage solution was collected and concentrated to dryness. Et₂O was added to the residue to precipitate the crude peptide, which was collected. The crude linear dicysteine containing peptide was purified by preparative RP-HPLC using a Waters XTerra prep RPdC8, 5 μm, 19 × 100 mm column, by Method 5 (see the [Supporting Information](#)). Next the peptide was cyclized by dissolution in H₂O and DMSO (9:1, v/v) in a concentration of approximately 2.5 mg of peptide mL⁻¹ and stirring the obtained solution at RT for 3 days. Subsequently, after lyophilization the cyclic peptide was purified using preparative RP-HPLC (0.10 g, 60% of yield) by Method 5 (see the [Supporting Information](#)). The purity of the peptides was evaluated by analytical UPLC using ACQUITY UPLC Peptide BEH C18 Column, 1.7 μm, 2.1 mm × 150 mm, H₂O/TFA 0.05% (A) and CH₃CN/TFA 0.05% (B) as eluents, by Method 6. Retention time 5.48 min for linear FibPep, Retention time 5.92 min for cyclic FibPep, purity of the peptides >90% (see the [Supporting Information](#)). ESI-MS (*m/z*): [M+2H]²⁺ 845.3 (obsd.), 845.1 (calcd. for linear FibPep C₇₂H₉₉CIN₁₆O₂₃S₃); [M+2H]²⁺ 844.0 (obsd.), 844.2 (calcd. for cyclic FibPep C₇₂H₉₇CIN₁₆O₂₃S₃).

Synthesis of FibPep-Gd-L2. SATA-FibPep (20 mg) was dissolved in 1 mL of water and 100 μL of 0.5 mol/L hydroxylamine hydrochloride, 25 mM EDTA solution were added to deprotect a thiol group and to yield the thiolated FibPep. The reaction was monitored by ESI (+)-MS and after stirring 2 h at RT the Sulfhydryl-FibPep was immediately recovered by HPLC separation (Method 5, see [Supporting Information](#)). [M+2H]²⁺ 822.9 (obsd.), 823.1 (calcd. for sulfhydryl-FibPep C₇₀H₉₅CIN₁₆O₂₂S₃). Then, sulfhydryl-FibPep (5.4 mg, 3.3 μmol) was dissolved in sodium acetate 50 mM, pH 6.0, 2 mL containing 30% acetonitrile and under argon atmosphere Gd-L2 (9.0 mg, 3 μmol) in 0.2 mL of water was added. The mixture was stirred at RT for 1 h and subsequently purified by gel permeation chromatography on a column packed with Sephadex G10 (1.1 × 12 cm), using Milli-Q H₂O as the mobile phase. After freeze-drying the product fractions, 11 mg (80% yield) of a white solid was obtained. ESI-MS (*m/z*): The purity of FibPep-Gd-L2 was evaluated by analytical UPLC using ACQUITY UPLC Peptide BEH C18 Column, 1.7 μm, 2.1 mm × 150 mm by Method 7, purity >85%. [M-4H]⁴⁻ 1153.6 (obsd.), 1153.6 (calcd. for C₁₇₁H₂₄₄ClGd₄N₃₇O₆₅S₃); [M-5H]⁵⁻ 922.5 (obsd.), 922.7 (calcd. for C₁₇₁H₂₄₄ClGd₄N₃₇O₆₅S₃).

Relaxometry. The longitudinal water proton relaxation rates were measured by using a Stellar SpinMaster relaxometer (Stellar, Mede (PV), Italy) operating at 0.5 T (21.5 MHz Proton Larmor Frequency), by mean of the standard inversion–recovery technique. The temperature was controlled with a Stellar VTC-91 air-flow heater equipped with a copper constantan thermocouple (uncertainty 0.1 °C). The proton 1/T₁ NMRD profiles were measured at 298 K on a fast field-cycling Stellar relaxometer over a continuum of magnetic field strengths from 0.00024 to 0.47 T (corresponding to 0.01–20 MHz proton Larmor Frequency). The relaxometer operates under computer control with an absolute uncertainty in 1/T₁ of ±1%. Additional data points in the range 21.5–70 MHz were obtained on the Stellar SpinMaster relaxometer. The concentration of the solutions used for the relaxometric characterization was determined according to a previously reported relaxometric method.⁴⁷ Briefly, the solution containing the

Gd(III)-complex is mineralized by transferring 0.1 mL of the Gd chelate solution into a sealable glass ampule, then bringing the volume to 0.2 mL with HCl 37% (analytical grade). The ampule is sealed and the solution heated at 120 °C for 18 h. The Gd(III) aquo-ion released is quantitated by measuring the water proton relaxation rate at 20 MHz and 25 °C (R_{1obs}), by the formula:

$$[\text{Gd}] = \frac{R_{1\text{obs}} - 0.5}{13.5} \quad (2)$$

where 13.5 is the relaxivity of free Gd(III) in acidic conditions, and 0.5 is the diamagnetic contribution to the relaxation rate, that is determined on a blank sample.

The concentration of Gd(III) ions in the fibrin plasma clots for the determination of relaxivity value at 20 MHz and 25 °C, was determined through ICP-MS analysis of the digested clots.

Binding to Fibrin Clots. Fibrin clots were prepared from human plasma (Sigma-Aldrich) as follows: Aliquots of 100 μL of plasma were freeze-dried and resuspended in solutions of Gd-L1pep with concentrations in the range 0.5–50 μM. To the plasma suspensions, 2 μL of calcium chloride (0.5 M) and 2 μL thrombin (100 U/mL) were added to reach the final concentrations of 10 mM and 2 U/mL, respectively. The samples were then incubated for 1 h at 37 °C during the formation of the clots. The experiments were carried out in triplicate. At the end of the incubation time, supernatant was carefully and completely removed, clots were weighed in order to calculate the clot volume (a density of 1 g/mL was considered), and 1 mL of HNO₃ 69% was added to the clots. After complete dissolution of the clots, samples were further digested by applying microwave heating (MicroSYNTH, Microwave labstation equipped with an optical fiber temperature control and HPR-1000/6 M six position high-pressure reactor, Milestone, Bergamo, Italy). After digestion, the volume of each sample was brought to 2 mL with ultrapure water, filtered with 0.45 μm filter, and analyzed by ICP-MS, using a Thermo Scientific ELEMENT 2 ICP-MS – Finnigan, Rodano (MI). The quantification was obtained through a calibration curve measured by using four gadolinium absorption standard solutions (Sigma-Aldrich) in the range 0.005–0.1 μg/mL. The concentration of fibrin-bound FibPep-Gd-L2 was calculated through the ratio between the total bound micromoles and the clot volume, while the concentration of the free FibPep-Gd-L2 was calculated as the difference with respect to the total micromoles in the incubation media divided by the incubation volume.

■ ASSOCIATED CONTENT

📄 Supporting Information

The Supporting Information is available free of charge on the [ACS Publications website](#) at DOI: [10.1021/acs.bioconjchem.8b00120](https://doi.org/10.1021/acs.bioconjchem.8b00120).

¹H NMR spectrum, 2D-TOCSY and 2D-NOESY, HPLC-UV/MS chromatograms, mass spectrum (ESI+) and ESI (–) of new compounds, preparative and analytical methods (PDF)

■ AUTHOR INFORMATION

Corresponding Author

*E-mail: rachele.stefania@unito.it. Telephone: +39-011-6706452. Fax: +39-011-6706487.

Notes

The authors declare no competing financial interest.

ACKNOWLEDGMENTS

This project has received funding from the EU's H2020 research and innovation program under the grant agreement No. 668142 (SPCCT) and AIRC Investigator Grant IG2013 No.14565 Dual MRI-Optical imaging agents in prostatectomy.

ABBREVIATIONS

NMR, nuclear magnetic resonance; MRI, magnetic resonance imaging; HPLC-MS, high performance liquid chromatography mass spectrometry; CA, contrast agents; AAZTA, 6-amino-6-methylperhydro-1,4-diazepinetetraacetic acid; PyBOP, benzotriazole-1-yl-oxy-tris-pyrrolidino-phosphonium hexafluorophosphate; DIPEA, *N,N*-diisopropylethylamine; HBTU, *O*-(benzotriazol-1-yl)-*N,N,N',N'* tetramethyluronium hexafluorophosphate; DMF, dimethylformamide; DCM, dichloromethane; TFA, trifluoroacetic acid; *t*Bu, *tert*-butyl

REFERENCES

- (1) Schlomka, J., Roessl, E., Dorscheid, R., Dill, S., Martens, G., Istel, T., Bäumer, C., Herrmann, C., Steadman, R., Zeitler, G., et al. (2008) Experimental feasibility of multi-energy photon-counting K-edge imaging in pre-clinical computed tomography. *Phys. Med. Biol.* 53 (15), 4031.
- (2) Schirra, C. O., Brendel, B., Anastasio, M. A., and Roessl, E. (2014) Spectral CT: a technology primer for contrast agent development. *Contrast Media Mol. Imaging* 9 (1), 62–70.
- (3) Si-Mohamed, S., Bar-Ness, D., Sigovan, M., Cormode, D. P., Coulon, P., Coche, E., Vlassenbroek, A., Normand, G., Boussel, L., and Douek, P. (2017) Review of an Initial Experience with an Experimental Spectral Photon-Counting Computed Tomography System. *Nucl. Instrum. Methods Phys. Res., Sect. A* 873, 27.
- (4) Caravan, P., Ellison, J. J., McMurry, T. J., and Lauffer, R. B. (1999) Gadolinium (III) chelates as MRI contrast agents: structure, dynamics, and applications. *Chem. Rev.* 99 (9), 2293–2352.
- (5) Aime, S., Chiaussa, M., Digilio, G., Gianolio, E., and Terreno, E. (1999) Contrast agents for magnetic resonance angiographic applications: 1 H and 17 O NMR relaxometric investigations on two gadolinium (III) DTPA-like chelates endowed with high binding affinity to human serum albumin. *J. Biol. Inorg. Chem.* 4 (6), 766–774.
- (6) Martin, V. V., Ralston, W. R., Hynes, M. R., and Keana, J. F. W. (1995) Gadolinium(III) Di- and Tetrachelates Designed for in Vivo Noncovalent Complexation with Plasma Proteins: A Novel Molecular Design for Blood Pool MRI Contrast Enhancing Agents. *Bioconjugate Chem.* 6, 616–623.
- (7) Aime, S., Barge, A., Cabella, C., Crich, S. G., and Gianolio, E. (2004) Targeting cells with MR imaging probes based on paramagnetic Gd (III) chelates. *Curr. Pharm. Biotechnol.* 5 (6), 509–518.
- (8) Aime, S., Castelli, D. D., Crich, S. G., Gianolio, E., and Terreno, E. (2009) Pushing the sensitivity envelope of lanthanide-based magnetic resonance imaging (MRI) contrast agents for molecular imaging applications. *Acc. Chem. Res.* 42 (7), 822–831.
- (9) Weissleder, R., and Mahmood, U. (2001) Molecular imaging. *Radiology* 219 (2), 316–333.
- (10) Aime, S., Cabella, C., Colombatto, S., Geninatti Crich, S., Gianolio, E., and Maggioni, F. (2002) Insights into the use of paramagnetic Gd (III) complexes in MR-molecular imaging investigations. *Journal of magnetic resonance imaging* 16 (4), 394–406.
- (11) Wiener, E. C., Konda, S., Shadron, A., Brechbiel, M., and Gansow, O. (1997) Targeting dendrimer-chelates to tumors and tumor cells expressing the high-affinity folate receptor. *Invest. Radiol.* 32 (12), 748–54.
- (12) Zhang, Z., Greenfield, M. T., Spiller, M., McMurry, T. J., Lauffer, R. B., and Caravan, P. (2005) Multilocus binding increases the relaxivity of protein-bound MRI contrast agents. *Angew. Chem., Int. Ed.* 44, 6766–6769.
- (13) James, M. L., and Gambhir, S. S. (2012) A molecular imaging primer: modalities, imaging agents, and applications. *Physiol. Rev.* 92 (2), 897–965.
- (14) Hu, H., Arena, F., Gianolio, E., Boffa, C., Di Gregorio, E., Stefania, R., Orio, L., Baroni, S., and Aime, S. (2016) Mesoporous silica nanoparticles functionalized with fluorescent and MRI reporters for the visualization of murine tumors overexpressing $\alpha\beta3$ receptors. *Nanoscale* 8 (13), 7094–7104.
- (15) Langereis, S., Geelen, T., Grill, H., Strijkers, G. J., and Nicolay, K. (2013) Paramagnetic liposomes for molecular MRI and MRI-guided drug delivery. *NMR Biomed.* 26 (7), 728–744.
- (16) Aime, S., Calabi, L., Cavallotti, C., Gianolio, E., Giovenzana, G. B., Losi, P., Maiocchi, A., Palmisano, G., and Sisti, M. (2004) [Gd-AAZTA]³⁺: a new structural entry for an improved generation of MRI contrast agents. *Inorg. Chem.* 43 (24), 7588–7590.
- (17) Baranyai, Z., Uggeri, F., Giovenzana, G. B., Bényei, A., Brücher, E., and Aime, S. (2009) Equilibrium and kinetic properties of the lanthanoids (III) and various divalent metal complexes of the heptadentate ligand AAZTA. *Chem. - Eur. J.* 15 (7), 1696–1705.
- (18) Di Gregorio, E., Gianolio, E., Stefania, R., Barutello, G., Digilio, G., and Aime, S. (2013) On the fate of MRI Gd-based contrast agents in cells. Evidence for extensive degradation of linear complexes upon endosomal internalization. *Anal. Chem.* 85 (12), 5627–5631.
- (19) Kanda, T., Osawa, M., Oba, H., Toyoda, K., Kotoku, J. I., Haruyama, T., Takeshita, K., and Furui, S. (2015) High signal intensity in dentate nucleus on unenhanced T1-weighted MR images: association with linear versus macrocyclic gadolinium chelate administration. *Radiology* 275 (3), 803–809.
- (20) Campa, C., Uggeri, F., Paoletti, S., and Flamigni, A. (2008). U.S. Patent Application No. 12/528,685.
- (21) Gugliotta, G., Botta, M., and Tei, L. (2010) AAZTA-based bifunctional chelating agents for the synthesis of multimeric/dendrimeric MRI contrast agents. *Org. Biomol. Chem.* 8 (20), 4569–4574.
- (22) Gianolio, E., Ramalingam, K., Song, B., Kalman, F., Aime, S., and Swenson, R. (2010) Improving the relaxivity by dimerizing Gd-AAZTA: Insights for enhancing the sensitivity of MRI contrast agents. *Inorg. Chem. Commun.* 13 (5), 663–665.
- (23) Baskin, J. M., Prescher, J. A., Laughlin, S. T., Agard, N. J., Chang, P. V., Miller, I. A., and Bertozzi, C. R. (2007) Copper-free click chemistry for dynamic in vivo imaging. *Proc. Natl. Acad. Sci. U. S. A.* 104 (43), 16793–16797.
- (24) Manzoni, L., Belvisi, L., Arosio, D., Bartolomeo, M. P., Bianchi, A., Brioschi, C., Buonsanti, F., Cabella, C., Casagrande, C., and Civera, M. (2012) Synthesis of Gd and ⁶⁸Ga complexes in conjugation with a conformationally optimized RGD sequence as potential MRI and PET tumor-imaging probes. *ChemMedChem* 7 (6), 1084–1093.
- (25) Dubey, L. V., and Dubey, I. Y. (2005) Side reactions of onium coupling reagents BOP and HBTU in the synthesis of silica polymer supports. *Ukrainica bioorganica acta* 1, 13–19.
- (26) Overoye-Chan, K., Koerner, S., Looby, R. J., Kolodziej, A. F., Zech, S. G., Deng, Q., Chasse, J. M., McMurry, T. J., and Caravan, P. (2008) EP-2104R: A fibrin specific Gadolinium-based MRI Contrast Agent for detection of Thrombus. *J. Am. Chem. Soc.* 130, 6025–6039.
- (27) Nair, S. A., Kolodziej, A. F., Bhole, G., Greenfield, M. T., McMurry, T. J., and Caravan, P. (2008) Monovalent and Bivalent Fibrin-specific MRI Contrast Agents for Detection of Thrombus. *Angew. Chem., Int. Ed.* 47, 4918–4921.
- (28) Starmans, L. W. E., van Duijnhoven, S. M. J., Rossin, R., Berben, M., Aime, S., Daemen Mat, J. A. P., Klaas Nicolay, K., and Grill, H. (2013) Evaluation of ¹¹¹In-Labeled EPep and FibPep as Tracers for Fibrin SPECT Imaging. *Mol. Pharmaceutics* 10, 4309–4321.
- (29) Zhou, Z., Wu, X., Kresak, A., Griswold, M., and Lu, Z. R. (2013) Peptide targeted tripod macrocyclic Gd (III) chelates for cancer molecular MRI. *Biomaterials* 34 (31), 7683–7693.
- (30) Chaabane, L., Tei, L., Miragoli, L., Lattuada, L., von Wronski, M., Uggeri, F., Lorusso, V., and Aime, S. (2015) In vivo MR imaging of

fibrin in a neuroblastoma tumor model by means of a targeting Gd-containing peptide. *Molecular Imaging and Biology: MIB* 17 (6), 819.

(31) De León-Rodríguez, L. M., and Kovacs, Z. (2008) The synthesis and chelation chemistry of DOTA-peptide conjugates. *Bioconjugate Chem.* 19 (2), 391–402.

(32) Wu, X., Burden-Gulley, S. M., Yu, G. P., Tan, M., Lindner, D., Brady-Kalnay, S. M., and Lu, Z. R. (2012) Synthesis and evaluation of a peptide targeted small molecular Gd-DOTA monoamide conjugate for MR molecular imaging of prostate cancer. *Bioconjugate Chem.* 23 (8), 1548–1556.

(33) Gringeri, C. V., Menchise, V., Rizzitelli, S., Cittadino, E., Catanzaro, V., Dati, G., Chaabane, L., Digilio, G., and Aime, S. (2012) Novel Gd (III)-based probes for MR molecular imaging of matrix metalloproteinases. *Contrast Media Mol. Imaging* 7 (2), 175–184.

(34) Aime, S., Botta, M., Crich, S. G., Giovenzana, G., Pagliarin, R., Sisti, M., and Terreno, E. (1998) NMR relaxometric studies of Gd (III) complexes with heptadentate macrocyclic ligands. *Magn. Reson. Chem.* 36, S200–S208.

(35) Gugliotta, G., Botta, M., Giovenzana, G. B., and Tei, L. (2009) Fast and easy access to efficient bifunctional chelators for MRI applications. *Bioorg. Med. Chem. Lett.* 19 (13), 3442–3444.

(36) Aime, S., Botta, M., Geninatti Crich, S., Giovenzana, G. B., Jommi, G., Pagliarin, R., and Sisti, M. (1997) Synthesis and NMR studies of three pyridine-containing triaza macrocyclic triacetate ligands and their complexes with lanthanide ions. *Inorg. Chem.* 36 (14), 2992–3000.

(37) Aime, S., Gianolio, E., Corpillo, D., Cavallotti, C., Palmisano, G., Sisti, M., Giovenzana, G., and Pagliarin, R. (2003) Designing Novel Contrast Agents for Magnetic Resonance Imaging. Synthesis and Relaxometric Characterization of three Gadolinium (III) Complexes Based on Functionalized Pyridine-Containing Macrocyclic Ligands. *Helv. Chim. Acta* 86 (3), 615–632.

(38) Aime, S., Gianolio, E., Terreno, E., Giovenzana, G. B., Pagliarin, R., Sisti, M., Palmisano, G., Botta, M., Lowe, M.p., and Parker, D. (2000) Ternary Gd (III) L-HSA adducts: evidence for the replacement of inner-sphere water molecules by coordinating groups of the protein. Implications for the design of contrast agents for MRI. *JBIC, J. Biol. Inorg. Chem.* 5 (4), 488–497.

(39) Cohen, S. M., Xu, J., Radkov, E., Raymond, K. N., Botta, M., Barge, A., and Aime, S. (2000) Syntheses and relaxation properties of mixed gadolinium hydroxypyridinonate MRI contrast agents. *Inorg. Chem.* 39 (25), 5747–5756.

(40) Gianolio, E., Cabella, C., Colombo Serra, S., Valbusa, G., Arena, F., Maiocchi, A., Miragoli, L., Tedoldi, F., Uggeri, F., Visigalli, M., et al. (2014) B25716/1: a novel albumin-binding Gd-AAZTA MRI contrast agent with improved properties in tumor imaging. *JBIC, J. Biol. Inorg. Chem.* 19 (4–5), 715–726.

(41) Lipari, G., and Szabo, A. (1982) Model-free approach to the interpretation of nuclear magnetic resonance relaxation in macromolecules. 1. Theory and range of validity. *J. Am. Chem. Soc.* 104 (17), 4546–4559.

(42) Lipari, G., and Szabo, A. (1982) Model-free approach to the interpretation of nuclear magnetic resonance relaxation in macromolecules. 2. Analysis of experimental results. *J. Am. Chem. Soc.* 104 (17), 4559–4570.

(43) Tei, L., Gugliotta, G., Gambino, G., Fekete, M., and Botta, M. (2017) Developing High Field MRI Contrast Agents by Tuning the Rotational Dynamics: Bisoqua GdAAZTA-based Dendrimers. *Isr. J. Chem.* 57, 887–895.

(44) Fulton, D. A., O'Halloran, M., Parker, D., Senanayake, K., Botta, M., and Aime, S. (2005) Efficient relaxivity enhancement in dendritic gadolinium complexes: effective motional coupling in medium molecular weight conjugates. *Chem. Commun.*, 474–476.

(45) Zhang, Z., Kolodziej, A. F., Greenfield, M. T., and Caravan, P. (2011) Heteroditopic binding of Magnetic Resonance Contrast Agents for Increased Relaxivity. *Angew. Chem., Int. Ed.* 50, 2621–2624.

(46) Barge, A., Cravotto, G., Gianolio, E., and Fedeli, F. (2006) How to determine free Gd and free ligand in solution of Gd chelates. A technical note. *Contrast Media Mol. Imaging* 1 (5), 184–188.

(47) Arena, F., Singh, J. B., Gianolio, E., Stefania, R., and Aime, S. (2011) β -Gal Gene Expression MRI Reporter in Melanoma Tumor Cells. Design, Synthesis, and in Vitro and in Vivo Testing of a Gd(III) Containing Probe Forming a High Relaxivity, Melanin-Like Structure upon β -Gal Enzymatic Activation. *Bioconjugate Chem.* 22, 2625–2635.